Evaluating the Impact of Weather-Induced Sensor Occlusion on BEVFusion for 3D Object Detection

Sanjay Kumar¹, Tim Brophy¹, Eoin Martino Grua¹, Ganesh Sistu^{1,2}, Valentina Donzella³, Ciarán Eising¹

Abstract-Accurate 3D object detection is essential for automated vehicles to navigate safely in complex real-world environments. Bird's Eye View (BEV) representations, which project multi-sensor data into a top-down spatial format, have emerged as a powerful approach for robust perception. Although BEVbased fusion architectures have demonstrated strong performance through multimodal integration, the effects of sensor occlusions, caused by environmental conditions such as fog, haze, or physical obstructions, on 3D detection accuracy remain underexplored. In this work, we investigate the impact of occlusions on both camera and Light Detection and Ranging (LiDAR) outputs using the BEVFusion architecture, evaluated on the nuScenes dataset. Detection performance is measured using mean Average Precision (mAP) and the nuScenes Detection Score (NDS). Our results show that moderate camera occlusions lead to a 41.3% drop in mAP (from 35.6% to 20.9%) when detection is based only on the camera. On the other hand, LiDAR sharply drops in performance only under heavy occlusion, with mAP falling by 47.3% (from 64.7% to 34.1%), with a severe impact on longrange detection. In fused settings, the effect depends on which sensor is occluded: occluding the camera leads to a minor 4.1% drop (from 68.5% to 65.7%), while occluding LiDAR results in a larger 26.8% drop (to 50.1%), revealing the model's stronger reliance on LiDAR for the task of 3D object detection. Our results highlight the need for future research into occlusion-aware evaluation methods and improved sensor fusion techniques that can maintain detection accuracy in the presence of partial sensor failure or degradation due to adverse environmental conditions.

Index Terms—3D Object Detection, Sensor Fusion, Bird's Eye View Perception, Sensor Occlusion, Automated Driving

I. INTRODUCTION

Modern automated vehicles rely on multiple sensors for accurate 3D perception [1]. Cameras provide rich appearance cues, such as colour and texture, but lack direct depth information, making it difficult to estimate distances accurately [2]. In contrast, LiDAR offers precise geometric measurements and depth data, but produces sparse point clouds that lack the high-resolution detail and semantic richness of camera images [3]. Fusing these complementary modalities into a BEV representation has emerged as an effective strategy for robust 3D object detection [4]. Despite progress in BEV-based sensor fusion architectures, most models are still evaluated under ideal, occlusion-free conditions [5], [6]. However, in real-world deployments, sensor outputs are frequently degraded due to environmental factors. Cameras may be partially

occluded by dirt, raindrops, or smudges on the lens, while LiDAR signals can be disrupted by adverse weather conditions such as fog or heavy rain, which reduce the number of returned points and the perception range [7]. These occlusions can significantly degrade detection performance and pose safety risks if not addressed properly.

Previous work has only partially explored this issue. Xie et al. [8] investigate camera occlusions but do not consider LiDAR degradation for 3D object detection. Brophy et al. [9] analyse the impact of rain on camera-based detection but do not examine the effect of multimodal fusion or occlusion in the BEV-based domain. The effect of sensor-specific occlusions remains underexplored, particularly in the context of BEV fusion models. In this work, we systematically investigate the effect of occlusions on both camera and LiDAR sensors using the BEVFusion [10] architecture and the nuScenes dataset [11]. Camera occlusions are simulated using soiling masks from the Woodscape dataset [12] to replicate real-world lens obstructions. For LiDAR, we simulate occlusion by randomly dropping a proportion of the point cloud, mimicking the degradation caused by adverse weather conditions such as fog or rain. We evaluate detection performance using standard metrics, including Mean Average Precision (mAP) and nuScenes Detection Score (NDS), and analyse how different levels of occlusion affect each sensor individually.

The main contributions of this paper are:

- We simulate occlusions on both the camera (using the Woodscape soiled dataset) and LiDAR (via random point cloud dropout).
- We evaluate the impact of these occlusions on 3D object detection using the BEVFusion architecture and the nuScenes dataset.
- We analyse modality-specific and fused performance under occlusion, highlighting the limitations of current fusion models and motivating the need for occlusionaware fusion strategies.

The remainder of the paper is structured as follows: Section 2 reviews related work. Section 3 describes the nuScenes dataset and explains how the camera and LiDAR occlusions are applied. Section 4 outlines the methodology, including the BEVFusion model architecture and experimental setup. Section 5 presents the results of our experiments. Section 6 discusses key findings and future directions.

II. RELATED WORK

3D object detection has become a critical task in automated driving, with methods generally categorised by their sensor

¹Dept. of Electronic and Computer Engineering and the Data Driven Computer Engineering Research Centre, University of Limerick, Castletroy, Co. Limerick V94 T9PX, Ireland.

²Valeo Vision Systems, Tuam, Co. Galway H54 Y276, Ireland.

³Queen Mary University of London, Mile End Road, London E1 4NS, UK. Corresponding Author: Mr. Sanjay Kumar (kumar.sanjay@ul.ie).

inputs: camera-only, LiDAR-only, and multi-modal fusion of camera and LiDAR data.

A. Camera-Only Methods

Recent advances have shown that 3D detection is possible using only image data. Li et al. [13] and Xie et al. [14] are two prominent researchers who developed approaches that construct a BEV representation from multi-camera images to facilitate detection. Li et al. [13] introduce a spatiotemporal transformer that aggregates camera views into a unified BEV space. In contrast, Xie et al. [14] jointly perform 3D detection and map segmentation by projecting multi-view image features into a shared voxel-based BEV grid. These methods avoid explicit depth supervision but still achieve competitive accuracy using camera-only inputs. However, camera-only methods struggle with accurate depth estimation, especially in low-light, distant, or occluded scenes. Without direct depth sensing, their 3D localisation is less reliable in challenging driving conditions.

B. LiDAR-Only Methods

LiDAR-based approaches benefit from precise geometric information. Lang et al. [15] encodes point cloud data into a pseudo-image using vertical columns (pillars), allowing fast inference via 2D convolutions in BEV space. Yin et al. [16] further improve performance by adopting a centre-based detection framework, where object centres are predicted directly from BEV features, simplifying the regression pipeline and enhancing both accuracy and speed. However, LiDAR-only methods lack the rich semantic and texture information available in camera images, making it difficult to distinguish between visually similar objects and accurately interpret scene context, especially for small or distant objects.

C. Camera-LiDAR Fusion Methods

To leverage the complementary strengths of LiDAR geometry and camera semantics, various fusion-based approaches have been proposed. Chen et al. [17] introduce learnable spatial offsets to align pixel-level image features with 3D LiDAR representations, enhancing the fusion process in BEV. Xu et al. [18] build on this by selectively injecting camera semantics into point cloud features via adaptive attention, improving performance, particularly for small or distant objects. Bai et al. [19] present a more robust and flexible fusion strategy: it first generates initial 3D bounding boxes using LiDAR BEV features, then refines predictions through a transformer-based attention mechanism that softly integrates relevant camera information, making it resilient to sensor misalignment and poor lighting conditions. In contrast, Chen et al. [20] avoid the BEV representation altogether by using a transformer to fuse camera and LiDAR features directly into 3D space, enabling the end-to-end prediction of bounding boxes from multimodal data. Collectively, these methods demonstrate that tightly coupled and learnable fusion mechanisms significantly boost 3D detection performance.

D. Robustness under Adverse Weather and Occlusion

While recent fusion methods have advanced detection accuracy on clean benchmarks, robustness under adverse weather and occlusion has received comparatively less attention. Xie et al. [8] introduced a benchmark to evaluate camera-based BEV models under natural corruptions such as fog, snow, low light, and motion blur, showing that detection performance drops sharply and varies across architectures. Kumar et al. [21] studied occlusions caused by dirt, raindrops, and fog in camera inputs, demonstrating significant degradation in BEV perception and highlighting the benefit of incorporating LiDAR and radar for robustness. More recently, Wang et al. [22] proposed MSAFusion, a reinforcement learning-based adaptive BEV fusion framework that dynamically adjusts sensor weights and uses random modality dropout to improve resilience under adverse weather, validated on nuScenes and Radiate datasets. Collectively, these works emphasise that adverse conditions substantially affect perception, yet systematic robustness evaluations of established BEV fusion models remain limited.

E. Research Gap

Although extensive progress has been made in cameraonly, LiDAR-only, and fusion methods, these approaches are typically trained and evaluated on clean, unoccluded data. Prior robustness studies address camera-only degradations, but they do not systematically examine existing BEV fusion models under controlled sensor occlusion. To fill this gap, we apply structured occlusions to both camera and LiDAR inputs in nuScenes and evaluate the robustness of BEVFusion for 3D object detection in BEV space.

III. DATASET

We use the nuScenes dataset [11], a large-scale benchmark for automated driving comprising 1,000 urban driving scenes from Boston and Singapore. Each 20-second scene includes synchronised data from six cameras, five radars, and a 32-beam LiDAR, sampled at 2 Hz, with 3D annotations for multiple object classes. The dataset provides 28,130 training and 6,019 validation samples, along with detailed maps, ego-vehicle poses, and calibrated sensor parameters, making it ideal for BEV-based multi-sensor perception. We chose nuScenes over other datasets, such as KITTI [23] and Waymo [24], due to its 360° multi-sensor setup (including radar) and its diverse urban scenarios with varying weather and lighting conditions. In comparison, KITTI lacks radar and has only front-facing sensors in clear conditions, while Waymo also lacks radar and offers less variation in environment and lighting. While nuScenes offers the advantage of 360° calibrated sensor coverage, real deployments may involve partial fields of view or non-overlapping camera-LiDAR angles. This limitation is important, as fusion performance can degrade in the presence of blind spots or misalignment. Addressing such cases is part of our ongoing work, where we study occlusions applied to specific regions of the LiDAR field of view.

To investigate the impact of sensor occlusion on 3D object detection in BEV, we simulate occlusions on both

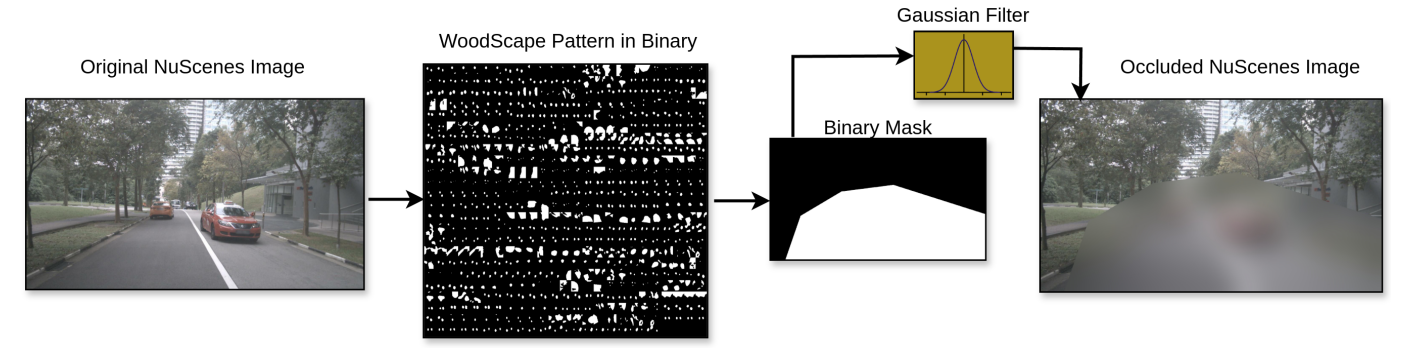


Fig. 1. From left to right: the original nuScenes image, followed by multiple binary occlusion patterns from the WoodScape soiling dataset. A randomly selected binary mask is smoothed using a Gaussian filter and applied to the original image to produce an occluded nuScenes image.

the camera and LiDAR modalities. For camera occlusion, we apply binary soiling masks derived from the Woodscape soiled dataset [12] to simulate real-world visual obstructions such as fog on the lens. For LiDAR, we simulate occlusion by randomly dropping a percentage of point cloud data, mimicking degradation caused by reduced visibility. These controlled degradations allow us to analyse the sensitivity of BEV-based detection architectures to real-world sensor challenges.

A. Simulated Camera Degradation

To simulate camera occlusion in the nuScenes dataset, as illustrated in Figure 1, we apply synthetic soiling patterns that resemble common visual degradations such as fog on the lens. These occlusion masks are derived from the Woodscape Soiled dataset, which provides a diverse set of contamination patterns observed in real driving conditions.

We begin by generating binary masks from these patterns to identify the regions of each camera image affected by occlusion. To simulate the visual distortion caused by lens contamination, we apply a Gaussian filter specifically to the masked areas. This replicates how fog blurs the visibility of the affected image regions while keeping the remaining image content intact.

Mathematically, the blurred occluded region I_{occluded} is computed as:

$$I_{\text{occluded}} = G_{\sigma} * (I \odot M)$$

where I is the original image, M is the binary occlusion mask (1 for occluded pixels, 0 elsewhere), \odot denotes element-wise multiplication, G_{σ} is a Gaussian kernel with standard deviation σ , and * represents the convolution operation.

The final occluded image I' is obtained by blending the blurred occluded regions with the clean parts of the image:

$$I' = I \odot (1 - M) + I_{\text{occluded}}$$

This method produces localised image degradation, preserving the global structure of the scene while impairing only the occluded areas. It enables a controlled study of how camera occlusion impacts BEV-based 3D object detection performance.

B. Simulated LiDAR Degradation

To investigate the effects of LiDAR occlusion on BEV-based 3D object detection, we simulate point cloud degradation in the nuScenes dataset by randomly removing a portion of LiDAR points from each frame, as shown in Figure 2. This random dropout mimics real-world scenarios in which LiDAR signals are partially lost due to environmental factors such as fog, storm, and rain. Given an input point cloud with N points, a fixed dropout ratio $r \in [0,1]$ is used to control the severity of degradation. The number of retained points is computed as:

$$N_{\text{retained}} = N \times (1 - r)$$

This method allows for controlled occlusion while avoiding spatial bias, as points are dropped uniformly at random across the scene. By varying r, we simulate different levels of occlusion severity and analyse the robustness of BEV-based detection models under degraded LiDAR input conditions. This approach aligns with Chan et al. [25], who simulate LiDAR occlusion by removing beams to model environmental noise factors like rain and partial lens blockage. We use simulated occlusions since nuScenes lacks sufficient severe fog, rain, or soiling cases for controlled analysis. Soiling masks and point dropout approximate these real-world degradations while allowing systematic and repeatable evaluation.

IV. METHODOLOGY

In this study, we evaluate the robustness of the BEVFusion [10] architecture under sensor occlusions to understand how degradation in camera and LiDAR inputs affects 3D object detection performance. We chose BEVFusion as it processes camera and LiDAR modalities independently, making it suitable for isolating occlusion effects, while remaining computationally efficient compared to newer transformer-based fusion models. BEVFusion is a state-of-the-art multi-sensor fusion framework that projects features from multiple modalities (camera and LiDAR) into a unified BEV representation. This allows effective fusion for the downstream perception task, i.e., 3D object detection.

A. Architecture Overview

BEVFusion transforms multi-view camera images and Li-DAR point clouds into a shared BEV space through steps

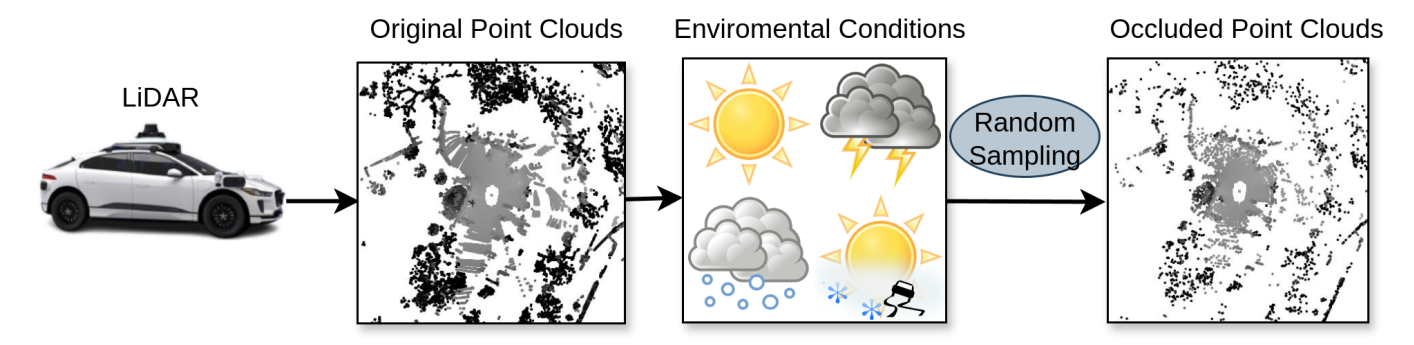


Fig. 2. From left to right: original nuScenes LiDAR point clouds, simulated environmental conditions (e.g., rain, fog, snow), a random sampling step that removes some LiDAR points, and the resulting occluded point clouds.

involving modality-specific encoders, view transformation to BEV space, BEV feature fusion, and task-specific prediction heads. As demonstrated in Figure 3, we describe each component in detail below:

1) Camera Encoder: Each input camera image is processed independently by a convolutional backbone, Swin-T [26], to extract 2D feature maps rich in semantic information. These features are further refined and merged across scales using a Feature Pyramid Network (FPS) [27], resulting in a unified multi-scale representation. The final output is a downsampled feature map of shape:

$$F^{\text{cam}} \in \mathbb{R}^{N \times H \times W \times C}$$

where N is the number of camera views, $H \times W$ is the spatial resolution of the feature map, and C is the number of feature channels.

2) LiDAR Encoder: Raw LiDAR point clouds are voxelized and passed through a 3D convolutional backbone, VoxelNet [28], to extract spatial features. The extracted LiDAR features are represented as:

$$F_{\mathrm{3D}}^{\mathrm{lidar}} \in \mathbb{R}^{X \times Y \times Z \times C}$$

where X, Y, Z are the voxel grid dimensions and C is the number of feature channels.

3) Camera-to-BEV View Transformation: The camera feature maps, originally in perspective view, are projected into 3D space using depth-aware lifting [27]. Specifically, each pixel feature is lifted along its camera ray into a set of D discrete depth bins. A depth distribution is predicted per pixel, and camera features are projected into 3D space according to:

$$F_{3D}^{\text{cam}}(x, y, z) = \sum_{d=1}^{D} p_d \cdot f_{(u, v, d)}$$

where p_d is the predicted probability for depth bin d, and $f_{(u,v,d)}$ is the lifted camera feature at pixel (u,v) and depth d. This operation generates a volumetric 3D feature representation from 2D image features.

4) BEV Pooling (Camera): The lifted 3D camera features are collapsed along the vertical (z) axis to form a 2D BEV

representation. BEVFusion uses sum pooling to aggregate features within each vertical column:

$$F_{\rm BEV}^{\rm cam}(x,y) = \sum_z F_{\rm 3D}^{\rm cam}(x,y,z)$$

This pooling strategy preserves the total feature magnitude within each grid cell and supports a dense accumulation of semantic features.

5) LiDAR-to-BEV Projection: Similarly, the 3D LiDAR features are projected into BEV by summing over the vertical axis. In practice, BEVFusion implements this via an efficient prefix sum over the voxelized features:

$$F_{\rm BEV}^{\rm lidar}(x,y) = \sum_z F_{\rm 3D}^{\rm lidar}(x,y,z)$$

This transformation aligns the LiDAR features to the BEV plane and prepares both modalities for spatially consistent fusion in the next stage.

6) BEV Feature Fusion: The BEV features from both modalities are concatenated to form a unified BEV representation:

$$F_{\mathrm{BEV}}^{\mathrm{fused}} = \mathcal{E}_{\mathrm{BEV}} \left(F_{\mathrm{BEV}}^{\mathrm{cam}} \oplus F_{\mathrm{BEV}}^{\mathrm{lidar}}
ight)$$

where \oplus denotes feature concatenation along the channel dimension, and \mathcal{E}_{BEV} is a fully convolutional BEV encoder. This encoder applies residual convolutional blocks to fuse the concatenated features and to mitigate any spatial misalignment between modalities.

- 7) Task-Specific Prediction Head: The fused BEV features are passed to task-specific heads for downstream 3D perception tasks. For 3D object detection, BEVFusion adopts a head structure inspired by [15] [18], which includes:
 - A center heatmap head to predict the 2D location of object centers in the BEV space.
 - Regression heads to estimate object attributes such as size, orientation, and velocity.

Each head is implemented as a lightweight convolutional block applied to the fused BEV feature map. These predictions are jointly supervised using standard object detection losses during training. Our setup utilises the pre-trained detection head provided by BEVFusion and evaluates its performance under various sensor occlusion settings without requiring retraining.

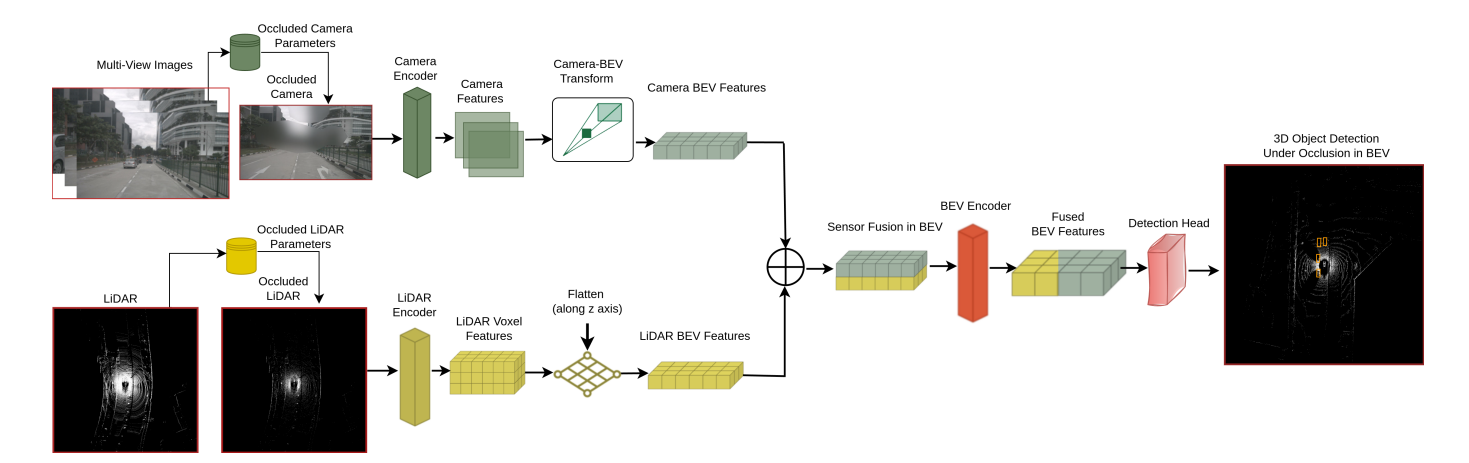


Fig. 3. Overview of the BEVFusion architecture used in our study. From left to right: multi-view camera and LiDAR inputs (including occluded variants) are encoded and transformed into BEV space, followed by sensor fusion, BEV encoding, and 3D object detection under occlusion.

8) Evaluation Under Sensor Occlusion: We evaluate the performance of the unmodified BEVFusion architecture on the nuScenes validation set under simulated sensor occlusions. Occlusions are applied to the camera and LiDAR inputs independently during inference, without retraining the model. The occlusion generation process, including Woodscape soiling masks for camera images and random point dropout for LiDAR, is described in detail in Section III. The goal is to assess the out-of-the-box robustness of BEVFusion to sensor degradation. Performance is measured using mean Average Precision (mAP) and nuScenes Detection Score (NDS), with analysis across different LiDAR occlusion levels.

V. EXPERIMENTAL RESULTS

A. Qualitative Results

1) LiDAR Occlusion with Clean Camera: We qualitatively evaluate the effect of LiDAR occlusion on 3D object detection performance while maintaining a clean camera input. The visualisation showcases detection results under different sensor configurations, with multi-view camera images on the left and corresponding BEV outputs on the right combined with LiDAR scan.

In Figure 4, the top row presents the ground truth for reference. When the camera and LiDAR are clean, the model successfully detects and localises objects in the scene with high precision. Following this, with clean camera input, the camera-only sensor (second row) cannot detect several objects due to the lack of depth cues, highlighting the limitations of vision-only perception. The third and fourth rows show predictions using LiDAR input only: the third row uses clean LiDAR data, while the fourth simulates occlusion by dropping 90% of LiDAR points. Although camera images are included in these two rows for visualisation purposes, they are not used during inference. These views help the reader better understand the layout of the scene and the positions of the objects, even though predictions are made solely from LiDAR data.

With clean LiDAR input alone (third row), the model maintains strong localisation accuracy, benefiting from precise spatial measurements. However, in the following row (fourth row), where LiDAR is progressively occluded by randomly dropping 90% of the point clouds, almost all objects are missed. As the distance between the object and the LiDAR sensor increases, the perception range decreases, becoming insufficient for reliable detection. Notably, in the fusion configuration (fifth row), where clean camera input is combined with 90% occluded LiDAR, the model consistently outperforms the LiDAR-only counterpart (d). The preserved visual features help compensate for the loss of geometric structure, allowing the model to detect missed objects in the LiDAR-only (d) configuration under occlusion. This demonstrates the effectiveness of BEVFusion's multi-modal design, which integrates camera semantics and LiDAR geometry into a unified BEV representation. Even under severe LiDAR degradation, the fusion framework enables more robust detection by leveraging complementary strengths from both modalities.

2) Camera Occlusion with Clean LiDAR: To evaluate the effect of camera degradation, we analyse detection performance when the camera input is occluded while the LiDAR input remains clean. The visualisation shows multi-view camera images on the left and BEV outputs on the right combined with LiDAR scan, comparing predictions across different sensor setups, i.e., camera and LiDAR.

In Figure 5, the top row shows the ground truth annotations for reference. The second row presents the output when only the camera input is used and kept clean. In this setting, the model can detect several objects using rich semantic features from the visual stream, but it struggles with accurate localisation, particularly for distant or partially occluded objects, due to the lack of depth information. The third row shows results when only the camera is used, and it is occluded. With no LiDAR input, detection performance drops significantly. Many objects are missed or inaccurately localised, especially those farther from the ego vehicle. This

TABLE I BEVFusion performance under increasing LiDAR occlusion (0%-90%) with clean camera input. Results compare LiDAR-only vs. Camera+LiDAR occlusion in terms of MAP and NDS.

Occluded Sensor	0	0%		30%		60%		70%		80%		90%	
	mAP	NDS											
LiDAR	64.68	69.28	62.58	67.98	56.94	64.38	54.65	62.96	48.06	58.80	34.09	49.62	
Camera + LiDAR	68.52	71.38	67.26	70.41	63.95	68.16	62.90	67.40	59.08	64.59	50.09	57.94	

Camera is Clean, LiDAR is Occluded

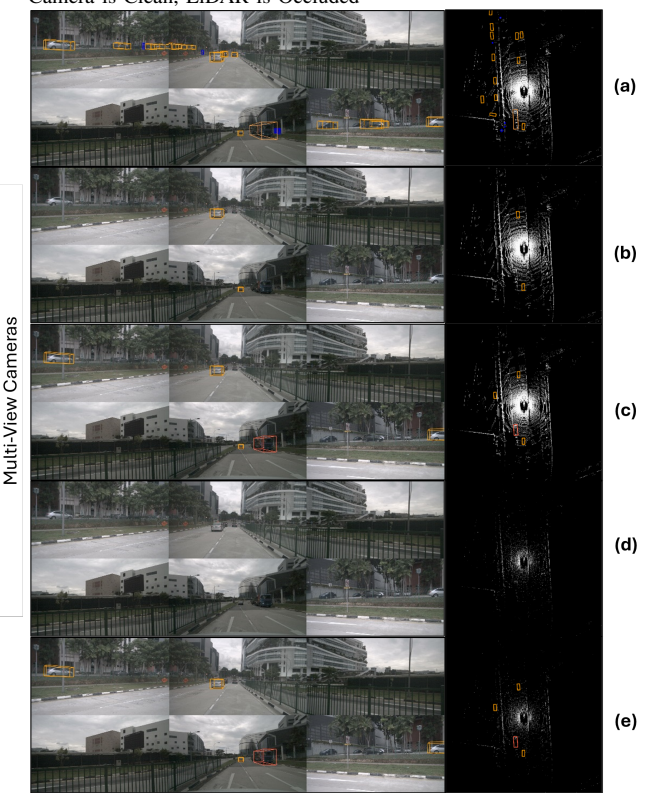


Fig. 4. Qualitative comparison of BEVFusion predictions under LiDAR occlusion. From top to bottom: (a) Ground truth, (b) Prediction with clean camera input, (c) Prediction with clean LiDAR input, (d) Prediction with occluded LiDAR, and (e) Prediction with clean camera + occluded LiDAR. For each row, the left images show the multi-view camera inputs, with the 3D detection predictions overlaid. The right image displays the input LiDAR scan, with the predictions overlaid in the BEV space.

highlights the vulnerability of vision-only models under adverse visual conditions. In the following rows, we analyse the fusion configuration where the camera is occluded but the LiDAR input remains clean. Despite visual degradation simulating real-world obstructions, such as fog, the model continues to detect and localise most objects accurately. This is due to the strong spatial information provided by the clean LiDAR sensor, which compensates for the missing or corrupted semantic features from the camera. These results confirm the robustness of the BEVFusion architecture under camera degradation when reliable LiDAR input is available.

3) Key Observation under LiDAR Occlusion: Figure 6 illustrates the impact of LiDAR occlusion on object detection across nearby frames. In (a), under heavy 90% LiDAR occlu-

sion, the model fails to detect any objects in the current frame, especially those at greater distances. In (b), fusing the same occluded LiDAR with clean camera input enables successful detection, highlighting the camera's contribution in recovering missed objects. In (c), using occluded LiDAR-only again, the previously undetected object becomes visible and is detected after five frames, once it moves closer to the ego vehicle. This reveals a key insight: under severe occlusion, LiDAR struggles with long-range detection but remains effective at short-range as objects approach, depending on the size and position of the occlusion. Overall, the figure demonstrates that camera input significantly enhances detection under LiDAR degradation, while LiDAR alone retains some utility for nearby objects.

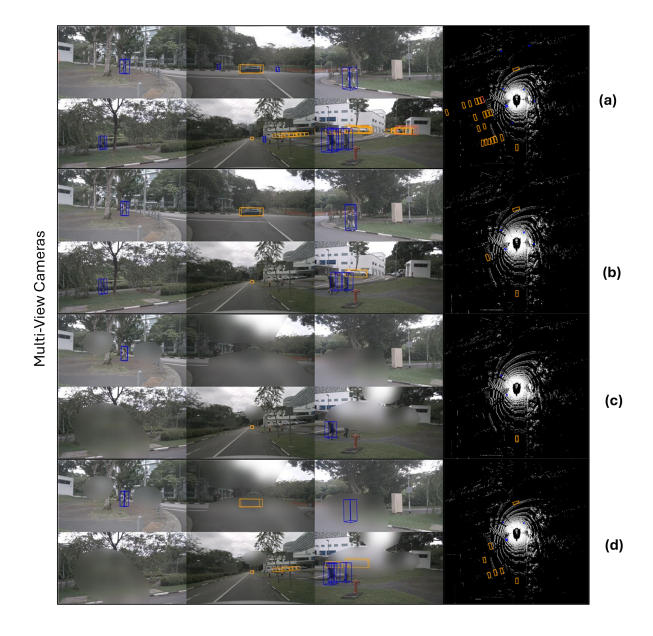


Fig. 5. Qualitative comparison of BEVFusion predictions under camera occlusion. (a) Ground truth, (b) Prediction with clean camera, (c) Prediction with occluded camera, and (d) Prediction with occluded camera + clean LiDAR. For each row, the left images show the multi-view camera inputs, with the 3D detection predictions overlaid. The right image displays the input LiDAR scan, with the predictions overlaid in the BEV space.

B. Quantitative Results

In this section, we present the quantitative analysis of our study, focusing on 3D object detection under camera and LiDAR occlusion, as shown in Table II. The BEVFusion architecture is used as the baseline, with results reported for both unoccluded and occluded sensor configurations. When using only the camera (C), the baseline model achieves



Fig. 6. Qualitative comparison across nearby frames, which highlights a key observation regarding LiDAR occlusion. Each row shows the six input camera images with overlaid 3D predictions: (a) LiDAR only input, with heavy occlusion applied. (b) LiDAR and camera input, with heavy occlusion applied to the LiDAR. (c) LiDAR only input, with the same heavy occlusion as (a), but applied to 5 samples later than previous rows.

35.6 mAP and 41.2 NDS. However, under camera occlusion, performance drops significantly to 20.9 mAP and 32.1 NDS, indicating the model's sensitivity to visual degradation. For the LiDAR-only setting (L), the baseline achieves significantly higher performance (64.7 mAP and 69.3 NDS), but under LiDAR occlusion (L-occluded), these metrics sharply decline to 34.1 mAP and 49.6 NDS. This severe drop corresponds to a 90% random dropout of LiDAR point clouds, used to simulate extreme weather conditions such as dense fog or heavy rain. Since 3D object detection relies heavily on accurate depth information from LiDAR, this drastic reduction in point density significantly impairs the model's ability to localise and identify objects in 3D space.

In the fusion configuration (C+L), BEVFusion achieves the best performance with 68.5 mAP and 71.4 NDS. When only the camera is occluded in the fusion setup, the drop in performance is minimal, with mAP decreasing slightly to 65.7 and NDS to 70.0. This indicates that the model can effectively rely on LiDAR data to compensate for missing visual information. In contrast, occluding the LiDAR in the fusion configuration results in a more pronounced performance loss, with mAP falling to 50.1 and NDS to 57.9. These results highlight the critical role of LiDAR in accurate 3D object detection and demonstrate that BEVFusion retains reasonable robustness under partial sensor occlusion, particularly when only the camera is degraded. LiDAR is more sensitive to occlusion because it depends on dense geometric points for 3D localisation; when many points are lost, the spatial structure collapses. Cameras, even when partly occluded, usually retain enough semantic context to sustain detection.

To further analyse the effect of LiDAR occlusion severity, we conducted experiments with 30%, 60%, 70%, 80%, and 90% point cloud dropouts. As shown in Table I, performance in the LiDAR-only setup remains relatively stable up to 60% occlusion (mAP drops from 64.68 to 56.94). However, beyond 70% occlusion, the drop becomes more significant, reaching 34.09 at 90%. This indicates that LiDAR remains fairly robust under moderate occlusion, but its reliability decreases sharply under severe degradation. In contrast, the sensor fusion setup (with a clean camera) maintains higher performance across all levels, with mAP dropping more gradually from 68.52 to 50.09. This demonstrates the benefit of multi-modal fusion, where clean camera input helps mitigate the impact of missing LiDAR data. This improvement is due to BEVFusion's ability to combine geometric information from LiDAR with semantic context from camera images in a shared BEV space. Even under severe LiDAR occlusion, the clean camera stream provides complementary cues that help maintain robust 3D detection.

TABLE II

PERFORMANCE COMPARISON OF BEVFUSION UNDER DIFFERENT SENSOR OCCLUSION SETTINGS. THE TABLE REPORTS MAP% AND NDS% FOR CLEAN SENSOR INPUTS, AS WELL AS FOR SCENARIOS WITH OCCLUDED CAMERA, OCCLUDED LIDAR, AND BOTH SENSORS COMBINED WITH OCCLUSION.

Method	Sensor	mAP%	NDS% 41.2 32.1	
BEVFusion [10] BEVFusion Occluded	C C-occluded	35.6 20.9		
BEVFusion [10] BEVFusion Occluded	L	64.7	69.3	
	L-occluded	34.1	49.6	
BEVFusion [10] BEVFusion Occluded BEVFusion Occluded	C+L	68.5	71.4	
	C+L (C-occluded)	65.7	70.0	
	C+L (L-occluded)	50.1	57.9	

VI. CONCLUSION AND FUTURE WORK

In this work, we presented a systematic study of the impact of sensor occlusions on 3D object detection performance within a BEV-based multi-sensor fusion framework. Using the BEVFusion architecture, trained on clean nuScenes data, we evaluated detection accuracy under two types of occlusions: camera degradation, simulated by soiling masks to replicate lens obstructions, and LiDAR degradation, achieved through random point cloud dropout to mimic visibility loss due to adverse weather conditions such as fog or rain. These occlusions were applied only during inference to isolate their individual and combined effects in a controlled setting. Our results show that camera-only models suffer significant performance drops even under moderate occlusion, while LiDAR-only models remain relatively robust up to 60% point dropout but degrade sharply beyond 70%. The fusion setup demonstrates higher resilience across all conditions, with clean input from one modality helping to compensate for occlusion in the other. These findings underscore the importance of occlusion-aware evaluation and motivate the development of more robust fusion strategies that can maintain reliable performance under partial sensor failure or environmental degradation. In future work, we plan to apply sensor occlusions not only during testing

but also during training, so the model can learn to handle degraded inputs more effectively. We also aim to explore the use of sequential frames (utilising temporal information) to help the model detect objects even when some sensors are momentarily occluded.

VII. ACKNOWLEDGMENTS

This work was supported with the financial support of the Science Foundation Ireland grant 13/RC/2094_P2 and co-funded under the European Regional Development Fund through the Southern & Eastern Regional Operational Programme to Lero - the Science Foundation Ireland Research Centre for Software (www.lero.ie)

REFERENCES

- [1] Gupta, Kajal, Adit Singhal, Ajit Kumar, and Pallab Maji. "Enhancing Sensor Perception: Integrating Multi-Sensor Data for Robust Sensor Perception." In 2025 17th International Conference on COMmunication Systems and NETworks (COMSNETS), pp. 78-83. IEEE, 2025.
- [2] Nawaz, Mehmood, Shehryar Khan, Muhammad Daud, Muhammad Asim, Ghazanfar Ali Anwar, Ali Raza Shahid, Ho-Pui Ho, Tom Chan, Daniel Pak Kong, and Wu Yuan. "Improving Autonomous Vehicle Cognitive Robustness in Extreme Weather with Deep Learning and Thermal Camera Fusion." IEEE Open Journal of Vehicular Technology (2025).
- [3] Qi, Yuanfan, Chun Liu, Marco Scaioni, Yanyi Li, Yihong Qiao, Xi-aolong Ma, Hangbin Wu, Keke Zhang, and Dazhi Wang. "Geometric information constraint 3D object detection from LiDAR point cloud for autonomous vehicles under adverse weather." Transportation research part C: emerging technologies 161 (2024): 104555.
- [4] Wen, Li-Hua, and Kang-Hyun Jo. "Fast and accurate 3D object detection for lidar-camera-based autonomous vehicles using one shared voxelbased backbone." IEEE access 9 (2021): 22080-22089.
- [5] Chen, Xuanyao, Tianyuan Zhang, Yue Wang, Yilun Wang, and Hang Zhao. "Futr3d: A unified sensor fusion framework for 3d detection." In proceedings of the IEEE/CVF conference on computer vision and pattern recognition, pp. 172-181. 2023.
- [6] Bai, Xuyang, Zeyu Hu, Xinge Zhu, Qingqiu Huang, Yilun Chen, Hongbo Fu, and Chiew-Lan Tai. "Transfusion: Robust lidar-camera fusion for 3d object detection with transformers." In Proceedings of the IEEE/CVF conference on computer vision and pattern recognition, pp. 1090-1099. 2022.
- [7] Espineira, Juan P., Jonathan Robinson, Jakobus Groenewald, Pak Hung Chan, and Valentina Donzella. "Realistic LiDAR with noise model for real-time testing of automated vehicles in a virtual environment." IEEE Sensors Journal 21, no. 8 (2021): 9919-9926.
- [8] Xie, Shaoyuan, Lingdong Kong, Wenwei Zhang, Jiawei Ren, Liang Pan, Kai Chen, and Ziwei Liu. "Robobev: Towards robust bird's eye view perception under corruptions." arXiv preprint arXiv:2304.06719 (2023).
- [9] GEEVER, DIARMAID, TIM BROPHY, DARA MOLLOY, ENDA WARD, BRIAN DEEGAN, MARTIN GLAVIN, and EDWARD JONES. "A Study on the Impact of Rain on Object Detection for Automotive Applications." IEEE Open Journal of Vehicular Technology (2025).
- [10] Liu, Zhijian, Haotian Tang, Alexander Amini, Xinyu Yang, Huizi Mao, Daniela L. Rus, and Song Han. "Bevfusion: Multi-task multi-sensor fusion with unified bird's-eye view representation." In 2023 IEEE international conference on robotics and automation (ICRA), pp. 2774-2781. IEEE, 2023.
- [11] Caesar, Holger, Varun Bankiti, Alex H. Lang, Sourabh Vora, Venice Erin Liong, Qiang Xu, Anush Krishnan, Yu Pan, Giancarlo Baldan, and Oscar Beijbom. "nuscenes: A multimodal dataset for autonomous driving." In Proceedings of the IEEE/CVF conference on computer vision and pattern recognition, pp. 11621-11631. 2020.
- [12] Yogamani, Senthil, Ciarán Hughes, Jonathan Horgan, Ganesh Sistu, Padraig Varley, Derek O'Dea, Michal Uricár et al. "Woodscape: A multi-task, multi-camera fisheye dataset for autonomous driving." In Proceedings of the IEEE/CVF International Conference on Computer Vision, pp. 9308-9318. 2019.

- [13] Li, Z., W. Wang, H. Li, E. Xie, C. Sima, T. Lu, Q. Yu, and J. Dai. "BEVFormer: Learning Bird's-Eye-View Representation from Multi-Camera Images via Spatiotemporal Transformers. arXiv 2022." arXiv preprint arXiv:2203.17270.
- [14] Xie, Enze, Zhiding Yu, Daquan Zhou, Jonah Philion, Anima Anandkumar, Sanja Fidler, Ping Luo, and Jose M. Alvarez. "M² BEV: multicamera joint 3D detection and segmentation with unified birds-eye view representation." arXiv preprint arXiv:2204.05088 (2022).
- [15] Lang, Alex H., Sourabh Vora, Holger Caesar, Lubing Zhou, Jiong Yang, and Oscar Beijbom. "Pointpillars: Fast encoders for object detection from point clouds." In Proceedings of the IEEE/CVF conference on computer vision and pattern recognition, pp. 12697-12705. 2019.
- [16] Yin, Tianwei, Xingyi Zhou, and Philipp Krahenbuhl. "Center-based 3d object detection and tracking." In Proceedings of the IEEE/CVF conference on computer vision and pattern recognition, pp. 11784-11793 2021
- [17] Chen, Zehui, Zhenyu Li, Shiquan Zhang, Liangji Fang, Qinghong Jiang, Feng Zhao, Bolei Zhou, and Hang Zhao. "Autoalign: Pixel-instance feature aggregation for multi-modal 3d object detection." arXiv preprint arXiv:2201.06493 (2022).
- [18] Xu, Shaoqing, Dingfu Zhou, Jin Fang, Junbo Yin, Zhou Bin, and Liangjun Zhang. "Fusionpainting: Multimodal fusion with adaptive attention for 3d object detection." In 2021 IEEE International Intelligent Transportation Systems Conference (ITSC), pp. 3047-3054. IEEE, 2021.
- [19] Bai, Xuyang, Zeyu Hu, Xinge Zhu, Qingqiu Huang, Yilun Chen, Hongbo Fu, and Chiew-Lan Tai. "Transfusion: Robust lidar-camera fusion for 3d object detection with transformers." In Proceedings of the IEEE/CVF conference on computer vision and pattern recognition, pp. 1090-1099. 2022.
- [20] Chen, Xuanyao, Tianyuan Zhang, Yue Wang, Yilun Wang, and Hang Zhao. "Futr3d: A unified sensor fusion framework for 3d detection." In Proceedings of the IEEE/CVF conference on computer vision and pattern recognition, pp. 172-181. 2023.
- [21] Kumar, Sanjay, Hiep Truong, Sushil Sharma, Ganesh Sistu, Tony Scanlan, Eoin Grua, and Ciarán Eising. "Minimizing Occlusion Effect on Multi-View Camera Perception in BEV with Multi-Sensor Fusion." arXiv preprint arXiv:2501.05997 (2025).
- [22] Wang, Mingchen, Hai Wang, Yicheng Li, Long Chen, Yingfeng Cai, and Zhen Shao. "MSAFusion: Object Detection Based on Multi-Sensor Adaptive Fusion under BEV." IEEE Transactions on Instrumentation and Measurement (2025).
- [23] Geiger, Andreas, Philip Lenz, Christoph Stiller, and Raquel Urtasun. "Vision meets robotics: The kitti dataset." The international journal of robotics research 32, no. 11 (2013): 1231-1237.
- [24] Sun, Pei, Henrik Kretzschmar, Xerxes Dotiwalla, Aurelien Chouard, Vijaysai Patnaik, Paul Tsui, James Guo et al. "Scalability in perception for autonomous driving: Waymo open dataset." In Proceedings of the IEEE/CVF conference on computer vision and pattern recognition, pp. 2446-2454, 2020.
- [25] Chan, Pak Hung, Gunwant Dhadyalla, and Valentina Donzella. "A framework to analyze noise factors of automotive perception sensors." IEEE Sensors Letters 4, no. 6 (2020): 1-4.
- [26] Liu, Ze, Yutong Lin, Yue Cao, Han Hu, Yixuan Wei, Zheng Zhang, Stephen Lin, and Baining Guo. "Swin transformer: Hierarchical vision transformer using shifted windows." In Proceedings of the IEEE/CVF international conference on computer vision, pp. 10012-10022. 2021.
- [27] Lin, Tsung-Yi, Piotr Dollár, Ross Girshick, Kaiming He, Bharath Hariharan, and Serge Belongie. "Feature pyramid networks for object detection." In Proceedings of the IEEE conference on computer vision and pattern recognition, pp. 2117-2125. 2017.
- [28] Yan, Yan, Yuxing Mao, and Bo Li. "Second: Sparsely embedded convolutional detection." Sensors 18, no. 10 (2018): 3337.
- [29] Philion, Jonah, and Sanja Fidler. "Lift, splat, shoot: Encoding images from arbitrary camera rigs by implicitly unprojecting to 3d." In Computer Vision–ECCV 2020: 16th European Conference, Glasgow, UK, August 23–28, 2020, Proceedings, Part XIV 16, pp. 194-210. Springer International Publishing, 2020.